Available online at www.sciencedirect.com

ScienceDirect

journal homepage: www.elsevier.com/locate/he

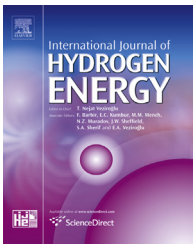

Optimization of a thermoelectric generator subsystem for high temperature PEM fuel cell exhaust heat recovery

Xin Gao, Søren Juhl Andreasen, Søren Knudsen Kær*, Lasse Aistrup Rosendahl*

Department of Energy Technology, Aalborg University, Pontoppidanstræde 101, Aalborg DK-9220, Denmark

ARTICLE INFO

Article history:
Received 17 September 2013
Received in revised form
26 January 2014
Accepted 27 January 2014
Available online 20 February 2014

Keywords:
TEG subsystem
Fuel cell
Heat recovery
Heat exchanger
Electrical connection
Optimization

ABSTRACT

In previous work, a thermoelectric (TE) exhaust heat recovery subsystem for a high temperature polymer electrolyte membrane (HT-PEM) fuel cell stack was developed and modeled. Numerical simulations were conducted and have identified an optimized subsystem configuration and 4 types of compact heat exchangers with superior performance for further analysis.

In this work, the on-design performances of the 4 heat exchangers are more thoroughly assessed on their corresponding optimized subsystem configurations. Afterward, their off-design performances are compared on the whole working range of the fuel cell stack. All through this study, different electrical connection styles of all the thermoelectric generator (TEG) modules in the subsystem and their influences are also discussed. In the end, the subsystem configuration is further optimized and a higher subsystem power output is achieved. All TEG modules are now connected into branches. The procedures of designing and optimizing this TE exhaust heat recovery subsystem are drawn out. The contribution of TE exhaust heat recovery to the HT-PEM fuel cell power system is preliminarily concluded. Its feasibility is also discussed.

1. Introduction

Fuel cells are considered as a cornerstone of the approaching hydrogen economy [1,2]. Among other fuel cell technologies, high temperature polymer electrolyte membrane (HT-PEM) fuel cells, operating around 160 °C, offers promising market potential [3–5]. Thanks to the increased operating temperature, they have better fuel impurity tolerance and easier cooling (greater temperature differences versus ambient air), in turn much simpler system configuration and possibility of high system efficiencies [6,7]. Yet another benefit of the relatively high operating temperature, the HT-PEM fuel cell exhaust heat is of higher quality and easier to utilize as process heat or recycle. To recover the exhaust heat for electricity and further boost the system efficiency, a thermoelectric (TE) exhaust heat recovery subsystem has already been introduced to the cathode exhaust of the fuel cell stack in a previous work [8].

In the previous work [8], the subsystem architecture was decided, model was made, and configuration was

* *Corresponding authors*. Tel.: +45 21370579; fax: +45 98151411.
E-mail addresses: xga@et.aau.dk (X. Gao), skk@et.aau.dk (S.K. Kær).

0360-3199/$ – see front matter Copyright © 2014, Hydrogen Energy Publications, LLC. Published by Elsevier Ltd. All rights reserved.
http://dx.doi.org/10.1016/j.ijhydene.2014.01.193

Table 1 – -Main equations [8,10].

Description	Equations
TEG properties	$\sum^{n_{x,TE}}\sum^{n_{y,TE}}\alpha_i=\alpha_{TE},\ \sum^{n_{x,TE}}\sum^{n_{y,TE}}R_{e,i}=R_{TE,e},\ \sum^{n_{x,TE}}\sum^{n_{y,TE}}R_{t,i}=R_{TE,t}$
TEG power output	$I_i=0.5(\alpha_i)-(\overline{T}_{h,TE}(i)\overline{T}_{c,TE}(i))/R_{e,i}$ $w(i)=\alpha_i I_i(\overline{T}_{h,TE}(i)-\overline{T}_{c,TE}(i))-I_i^2R_{e,i},\ P_{TEA}=\sum^{nx}n_x\sum^{ny}n_y w(i)$
Heat transfer	$\dot{q}_{h,TE}(i)=\dot{q}_{gas}(i)=\dot{m}_{gas}(h_{gas,i}-h_{gas,i+1})$ $\dot{q}_{gas}(i)=\varepsilon_{ctf}(i)\dot{m}_{gas}(h_{gas,i}-h^{cw}_{gas,i})$ $\dot{q}_{h,TE}(i)=UA_{hx}(i)(\overline{T}_{gas}(i)-\overline{T}_{h,TE}(i)),\ \overline{T}_{gas}(i)=(T_{gas}(i)+T_{gas}(i+1))/2$
Pressure drop	$\Delta p_{hx}=(u^2_{gas}/(2\rho_{gas,in}))[4f_{hx}L_{hx}\rho_{gas,in}/(D_h\overline{\rho}_{gas})+(1+\sigma^2)((\rho_{gas,in}/\rho_{gas,out})-1)]$

preliminarily optimized. As illustrated in Fig. 1, the subsystem is constructed in a way similar to a compact plate-fin gas–liquid heat exchanger. Part No. 3 is the compact heat exchanger housing for the fuel cell stack exhaust gas, which works as the heat source. Part No. 1&4 are two aluminum blocks with a liquid coolant circulating inside, as the heat sink. The coolant is actually a methanol–water mixture, which is stored in a tank primarily as fuel and will be gradually reformed into hydrogen for the fuel cell stack [9]. Thermoelectric generator (TEG) modules, namely part No. 2, are interposed between the aforementioned two parts. As a whole, these parts form the sandwich structure subsystem. The subsystem was then modeled using a finite-element approach with higher precision and better versatility for both design-type and simulation-type problems. Main equations are presented in Table 1. On the model, a sensitivity analysis was carried out and has identified the subsystem main variables. In the end, the subsystem configuration was optimized. There were 6 TEG modules crossing the exhaust gas flow by 7 modules along the flow. They together scale the subsystem size. All the modules were electrically in series. On this optimized configuration, 4 types of heat exchangers with superior performance were also identified.

In this work, instead of keeping the subsystem size invariant in all cases, it is adjusted correspondingly to each of the 4 chosen heat exchangers to more properly assess their performances. Besides the above on-design performance optimization under the same fixed fuel cell stack operating point as in the previous work, research is also carried out on the whole working range of the stack. It is the off-design performance optimization. Another factor that evidently affects the subsystem performance, the electrical connection styles of TEG modules, is also more thoroughly investigated in this work. Finally, the further optimized subsystem is depicted; a more efficient and practical electrical connection scenario of all the TEG modules is proposed; the procedures of designing and optimizing the TEG subsystem are generalized. At the end of this work, the contribution and perspectives of the TE exhaust heat recovery to the HT-PEM fuel cell power system are also discussed.

2. On-design performance optimization

In this paper, all simulation settings not explicitly given are corresponding with the previous work [8] and 'the subsystem power output' refers in particular to its maximum value. The 4 types of heat exchangers studied here were identified by their outstandingly low pressure drop still with high heat transfer performance. Table 2 lists their brief information. More details can be found in Ref. [11].

In this section, the on-design performances of 4 different subsystems denoted by their equipped heat exchangers are analyzed. The word "on-design" refers to the nominal working point of the HT-PEM fuel cell stack. The stack current density is fixed to ≈0.67 A/cm^2; the stack cathode stoichiometry is assumed to be around 19 [12,13]. To this nominal working condition, 4 subsystems are optimized respectively for determining the final optimal subsystem configuration. Results are as follows.

2.1. *Heat transfer process optimization*

To enhance the heat transfer process, the size of the subsystem needs to be optimized, which is scaled by the number of TEG modules crossing the exhaust gas flow and the number of modules along the flow, n_{cro} and n_{run}. Two steps are needed here: 1) finding out the candidate n_{cro}, and 2) choosing the optimum n_{cro} and n_{run}.

Before finding out the candidate n_{cro}, an adequate n_{run} for all the 4 heat exchangers needs to be identified. It requires, under any n_{cro} and any heat exchanger type, all possible exhaust heat will be always recovered by the subsystem. The minimum applicable n_{cro} of 2 is used to pinpoint the adequate n_{run}. For each heat exchanger, there is a smallest n_{run} when the subsystem power output varies less than 0.5% between n_{run} and $n_{run}-1$. Then the largest n_{run} among the four is the adequate n_{run}, which equals 26 in this study. Afterward, this n_{run} is kept invariant to identify the candidate n_{cro} for each of the 4 heat exchangers. Results are presented in the following figures.

Table 2 – The 4 types of heat exchangers [8].

Index	Name	Page no. in Ref. [11]
1	'Plain plate-fin, surface 15.08'	229
2	'Pin-fin plate-fin, surface PF-10(F)'	262
3	'Strip-fin plate-fin, surface 1/6-12.18(D)'	250
4	'Pin-fin plate-fin, surface PF-4(F)'	260

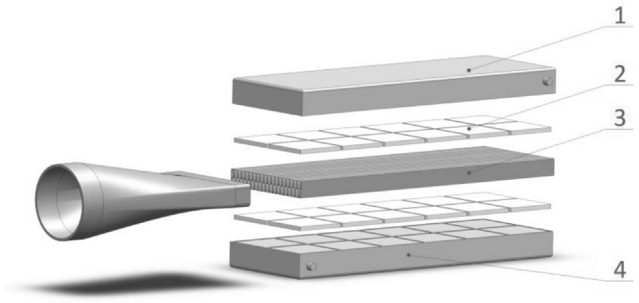

Fig. 1 – The architecture of the subsystem main body (1,4 – Aluminum blocks; 2 – TEG module assembly; 3 – Compact heat exchanger housing).

Fig. 2 shows the subsystem power output and its pressure drop changing with n_{cro} on each of the 4 heat exchangers. On the whole in all 4 cases, the subsystem power output drops monotonically with n_{cro} increasing and the trend becomes moderate in the second half range. The exception is the rise happening at the beginning in case 4. This is explained by the possible whistle problems and should be avoided in practice [11]. Considering the subsystem pressure drop in each case, there is a steep decrease in the first half range and then the effect of increasing n_{cro} fades out. It is clear the candidate n_{cro} is a tradeoff between the subsystem power output and its pressure drop [8]. In this study, the subsystem pressure drop is not allowed to go above 900 Pa. Constrained by this, the candidate n_{cro} for each heat exchanger can only be selected among 4, 6 and 8. The final choice is the result of the interplay between n_{cro} and n_{run}.

From Fig. 2, it can also be observed that the subsystem on the 4th heat exchanger has the highest power output and lowest pressure drop. It is also less sensitive to n_{cro}, as illustrated by Fig. 3. It is clearly shown that changing n_{cro} barely influences the power output compared to the other 3 types. This also means possible higher off-design performance of the 4th type. In a word, heat exchanger type 4 is probably the best choice. This will be more thoroughly examined in the following sections.

With the candidate n_{cro} prepared, the next step here is to identify the optimum n_{cro} and n_{run} for each heat exchanger. Calculations are still carried out for the subsystem power output and pressure drop on different heat exchangers, except now not only versus n_{cro} but also versus n_{run}. Results are plotted in Fig. 4. The 900 Pa criterion is the grey dash-dot line in each figure. It can be seen there is a peak power output for each subsystem setup but the pressure drop is nearly proportional to n_{run} on the whole range. Trends are quite similar to [14,15]. Under each setup, there is an intersection between the pressure drop curve and the 900 Pa line. It can be concluded that the final optimal subsystem configuration for each heat exchanger is the setup under which the subsystem reaches its highest peak power output point provided that the peak point comes before the intersection point. They are listed in Table 3. As shown, the subsystem installed with the 4th heat exchanger has the highest power output, the lowest press drop and the least number of TEG modules. It is most likely to be the final optimal subsystem configuration. Following study is carried out on it.

Throughout deciding Table 3, all TEG segments (fragments of the TEG modules from the finite-element discretization [8,10]) in the subsystem were electrically in series. Under this condition, the TEG subsystem has the lowest power output

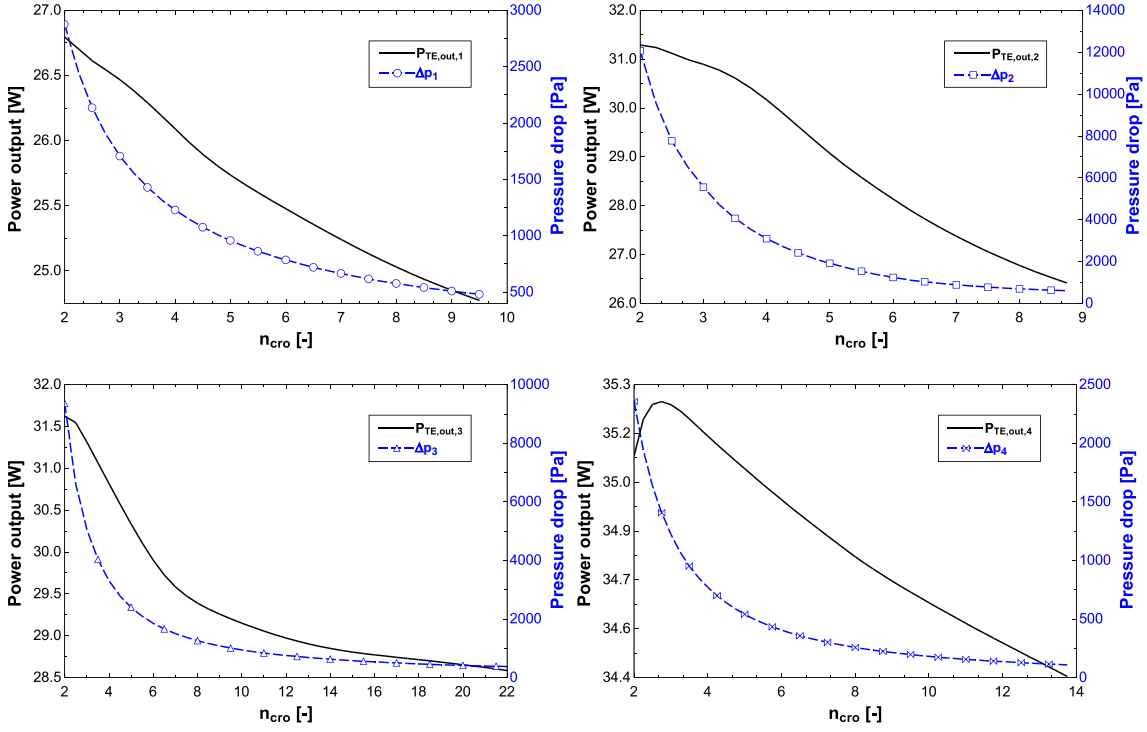

Fig. 2 – Subsystem power output and pressure drop vs. n_{cro} on different heat exchangers.

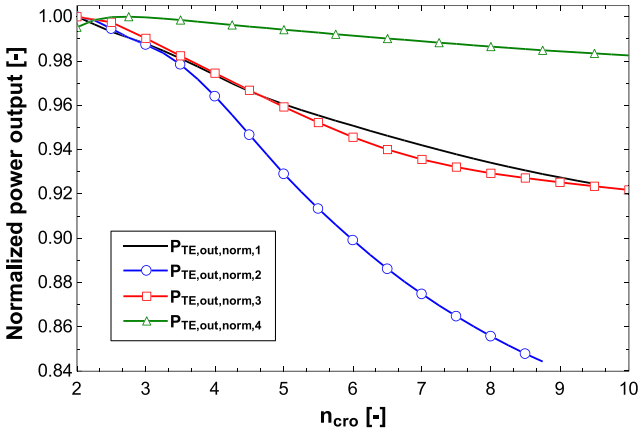

Fig. 3 – Normalized subsystem power output by the peak value of each heat exchanger.

and the worst reliability [16]. On the contrary, during determining the candidate n_{cro}, all TEG segments were kept working in standalone mode, i.e., each TEG segment is assumed connected with an external resistance equivalent to its internal. Under this condition, every TEG segment together with the subsystem has its maximum power output. It is a reasonable simplification in these calculations since it can avoid this electrical connection effect from interfering with deciding the candidate n_{cro}. However, the standalone mode is obviously lack of feasibility in practice. With the progress of power conditioning techniques [17–19], it is apparently more practical to divide all the TEG modules into branches. This electrical connection style affects the system design and performance.

2.2. *Electrical power output enhancement*

The demand of power conditioning for TEGs is based on two simple facts: 1) their maximum power point drifts significantly with their working temperature, as concluded by the sensitivity analysis in Refs. [8]; 2) series connection of all the TEG modules has the worst performance and reliability [16], as mentioned above. To alleviate these two issues, all the TEG modules of the subsystem will be electrically divided into branches. Since it is assumed that the subsystem performance in the direction perpendicular to the exhaust gas flow is identical [8], the TEG assembly will only evenly fall into branches along the flow in the following study. Inside each branch, all modules are electrically in series. Each branch is connected with a dedicated power conditioning circuit, i.e., branches work standalone, electrically independent from each other. The total number of branches n_b affects the subsystem performances. Analysis is carried out as follows.

Fig. 5 illustrates the effects of n_b with n_{run} on the subsystem power output on the 4th heat exchanger. Under every n_b, the subsystem power output overlaps and ascends fast initially, reaches the peaks and then starts to drop gradually. With larger n_b, the dropping trend becomes dimmer, i.e., the power output is less sensitive to n_{run}. The two curves of the standalone mode and the serial mode give the upper and lower bounds of the power output. It is notable from Fig. 5 that n_b stimulates the subsystem power output significantly. However, when there are more branches this effect becomes less significant. This phenomenon is illustrated quantitatively in

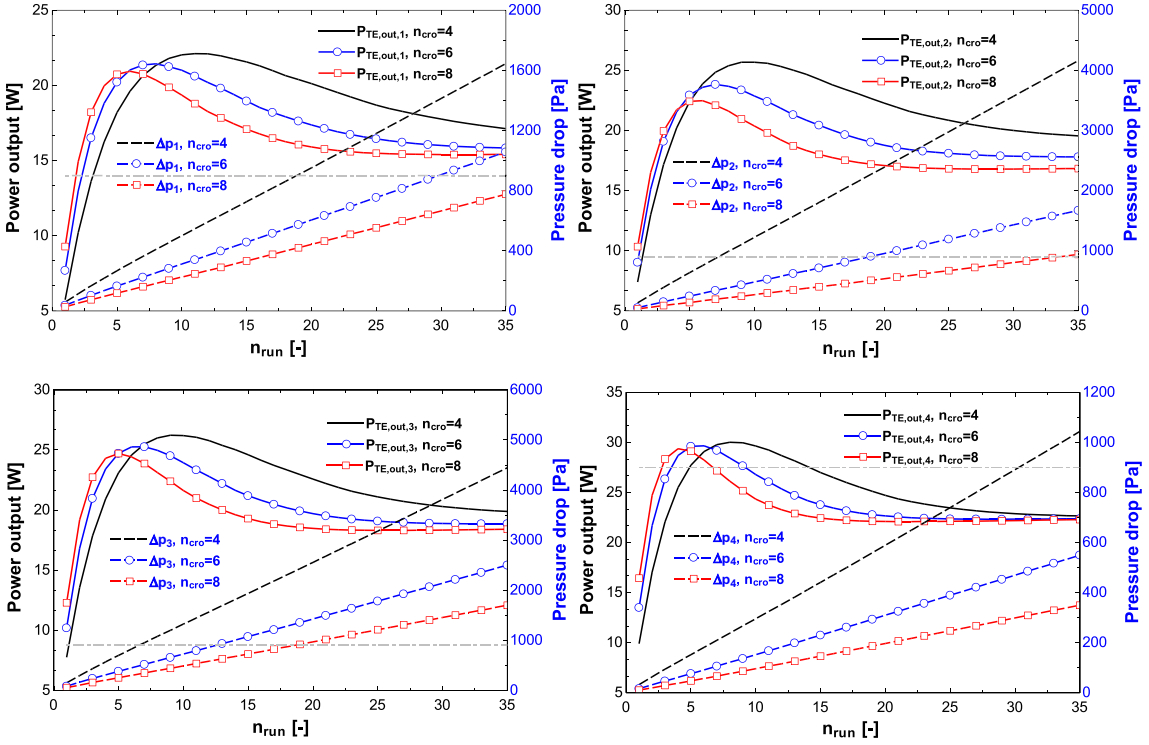

Fig. 4 – Subsystem power output and pressure drop vs. both n_{cro} and n_{run}.

Table 3 – The final optimal subsystem configurations.

Index[a]	n_{cro}	n_{run}	Power output [W]	Pressure drop [Pa]
1	4	11	22.12	545.95
2	6	7	23.83	337.43
3	6	7	25.27	520.72
4	4	8	30.01	238.17

[a] Corresponding to Table 2.

Table 4 by the normalized power output. As n_b changing from 1 to 2, the power output increases by 8.4%. Then the increment drops to 2.8% and 1.4%.

It can also be noticed that n_b encourages a larger n_{run} from Table 4 and Fig. 5. Balanced between the subsystem power output and pressure drop, the 3-branch combination is chosen as the final optimal configuration of the subsystem for the on-design working condition. Compared to the in-series configuration, this configuration can boost the subsystem power output by 12.9%. The improvement is then up to 40.6% over the optimized configuration in the previous work [8]! Still, the subsystem pressure drop is now 7.8% less.

3. Off-design performance optimization

In this section, the performances of the four configurations in Table 3 and the final on-design optimal configuration are assessed under off-design working conditions. "Off-design" means the fuel cell stack working mode changes in the whole operational range, off the abovementioned "on-design" nominal spot. According to [12,13,20], the operational current density range of the stack in this study is from 0 A/cm^2 to1 A/cm^2. To avoid fast degradation of the stack [21], the exhaust gas temperature is chosen as the control parameter and kept at 155 °C invariant in this study.

3.1. Assessment of the subsystem configurations

Fig. 6 shows the off-design performances of the four configurations in Table 3. Limited by the Reynolds-number operating interval of each heat exchanger [11], subsystem performance data are only available as presented in the figures. Outside of these intervals, compact heat exchangers will lose their advantages because their performances are no better than ordinary smooth-passage heat exchangers [11]. It can be seen that curves in Fig. 6 have similar trends as in Ref. [8]. Among them, the 4th configuration has the highest subsystem power output and lowest pressure drop on the whole range. It has higher performance and a wider operating interval. In other words, the 4th heat exchanger is still the ideal choice for the off-design operations. In the above study, all TE segments work in standalone mode.

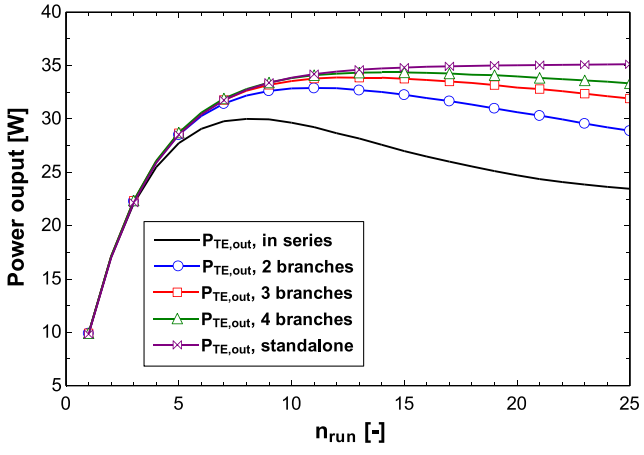

Fig. 5 – Effects of n_b with n_{run} on the 4th heat exchanger.

3.2. The final optimal configuration

The effect of power conditioning on the final on-design optimal configuration, the 4th combination in Table 3, under off-design operating conditions is illustrated below.

It is clearly illustrated in Fig. 7 the benefits of power conditioning for off-design operations. In the worst case, the final subsystem in the serial mode ($n_b = 1$) can only produce approximately 60% power as in the standalone mode. Under the same working condition, electrically dividing all the modules into three branches ($n_b = 3$) can improve the power output to about 80%. It is then nearly 90% when $n_b = 4$, which is about 30% higher than the serial mode! Since the fuel cell system mostly working in the second half operational range, balanced between the performance and system complexity $n_b = 3$ is still the preferable final choice. In this half range, dividing into three branches can guarantee no less than 96% power output. On the contrary, in the whole range the subsystem power output under the serial mode is typically less than 85%.

Furthermore, it can also be noticed in Fig. 7 that the normalized power output curve of the serial mode is slightly different from the others. It has milder power output drop at the low current density end. This is questionable since the curves are from the same subsystem configuration except only with n_b changed from 1 to 4. They should have similar trends. Checking the exhaust gas temperature distribution under two current densities $i = 0.25$ A/cm^2 and 0.67 A/cm^2 as shown in Fig. 8, it can be noticed that the downstream modules almost have no temperature difference on them under 0.25 A/cm^2. Large non-uniform temperature distribution between modules happens in the current subsystem. Electrically in series with the large non-uniformity, the downstream modules become under-temperature. It is the condition these TE modules working at much lower temperature differences regarding their output electric current. Since TEGs and thermoelectric coolers (TECs) are inherently twinborn working modes of a single TE module, these under-temperature modules probably have already shifted to the TEC mode. Then they act similarly as the TEC modules in the directly

Table 4 – Effects of n_b with n_{run} to the subsystem power output.

Connection Style[a]	n_b[a]	n_{run}[a]	$P_{TE,out}$ [W]	Normalized $P_{TE,out}$[b]	Pressure drop [Pa]
In series (1 branch)	4	8	30.01	0.87	238.17
2 branches	4	11	32.91	0.95	324.30
3 branches	4	12	33.88	0.98	353.24
4 branches	4	14	34.36	0.99	411.50

[a] The optimal subsystem configuration.
[b] Normalized by the standalone style.

coupled TEG–TEC systems in Refs. [22,23]. Instead of generating electricity, these modules are actually wasting it. Besides this TEC power dissipation, the internal ohmic resistances of these under-temperature modules can be counted as line loss and jointly reduce the system net power output. Without considering this shift possibility, the current subsystem model seems having overestimated the power output at the low current density end. Thanks to introducing power conditioning, this deviation is mitigated temporally.

The above possible TEG–TEC shift was rarely considered in TEG system-level modeling in literature. It seems TEC working mode should also be included in modeling a TEG system, especially when under-temperature phenomenon happens. This TEG-TEC shift also raises another necessity of power conditioning for TEG systems.

From all the above analyses, the final optimal configuration of the subsystem on its whole working range can be finally concluded. As shown in the following Fig. 9, there are 2 blocks, each with 2 rows of 12 TEG modules in the subsystem. As a total, there are 48 modules. They together decide the size of the subsystem including the heat exchanger housing. The type of the installed heat exchanger is 'Pin-fin plate-fin, surface PF-4(F)'. Its detailed geometry is given in Fig. 10. TEG module type is Melcor HT8 [8]. All the modules are electrically divided in 3 branches along the exhaust gas flow, as illustrated in different colors in the figure.

4. Contribution of TE heat recovery to the fuel cell system

On the final optimized TEG subsystem, the contribution of the TE heat recovery to the current 1 kW fuel cell power system is assessed.

Assume that there is no power loss during power conditioning, Fig. 11 shows the benefits of TE heat recovery to the fuel cell system. It raises the system power output, i.e., the system voltage or electric current is higher. From the normalized system power output, it can be seen the gain is around 3.5%. It should be mentioned that the figure of merit (ZT) of the TEG modules being used is fairly low. It is only around 0.50 [8,24]. Commonly, it can reach up to 0.8 to 1.1 in practice by tuning the carrier concentration of the module's materials or changing them [25]. However, it is widely agreed in the research community that for TEGs to be economically viable in most applications, ZT must have values of 2 or higher [26]. Refer to the achievements in the lab as shown in Refs. [27], this seems soon achievable.

Substitute ZT = 2 into the above calculation, the contribution of the TE heat recovery can be expected as Fig. 12. Now around 10% gain in the power output of the 1 kW fuel cell system is realized. This is extra 90.20 W power under its nominal operating condition, which is approximately 3 times as the condition ZT = 0.50. It is already able to be easily used to drive the auxiliaries, charge batteries, assist the system startup/shutdown processes, etc. For further system level study, the equations of the normalized power output (NPo) to the fuel cell stack operating current density (i) are given below. The unit of i is A/cm^2.

$$\mathrm{NPo} = \begin{cases} 1.010 + 0.045\cdot i - 0.011\cdot i^2, & \mathrm{ZT} = 0.50 \\ 1.032 + 0.104\cdot i - 0.020\cdot i^2, & \mathrm{ZT} = 2.0 \end{cases} \quad (1)$$

5. Conclusions

The configuration of the TEG exhaust heat recovery subsystem is further optimized. There are 4 x 12 TEG modules in the

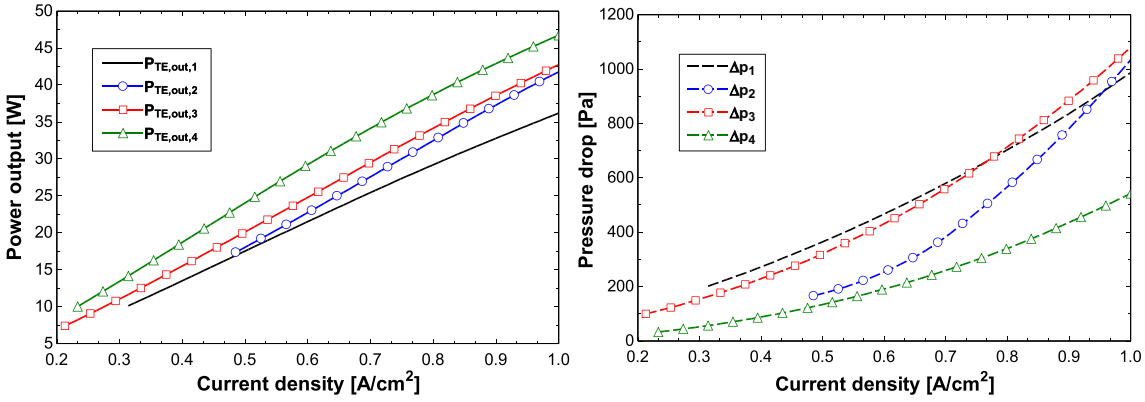

Fig. 6 – The off-design performances of the 4 configurations in Table 3.

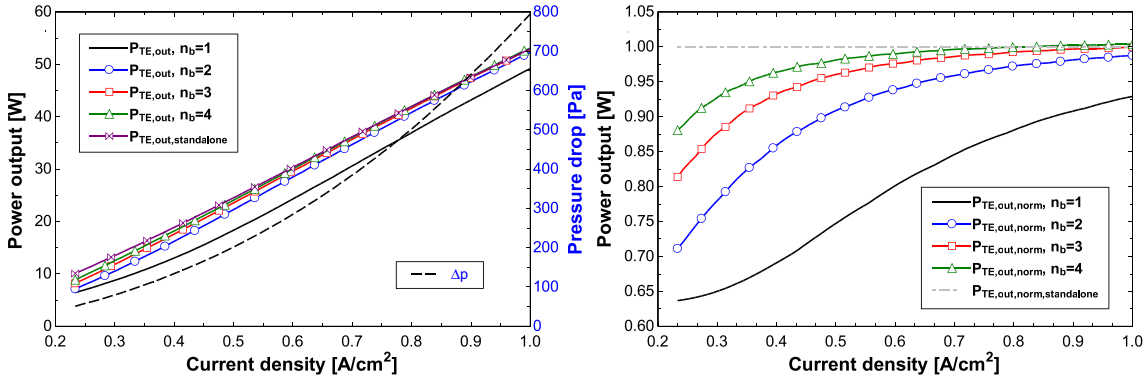

Fig. 7 – The off-design performances of the final optimal configuration.

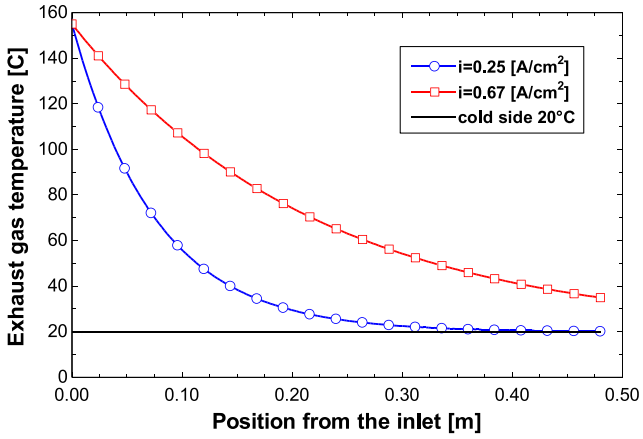

Fig. 8 – Exhaust gas temperature distribution under two different current densities.

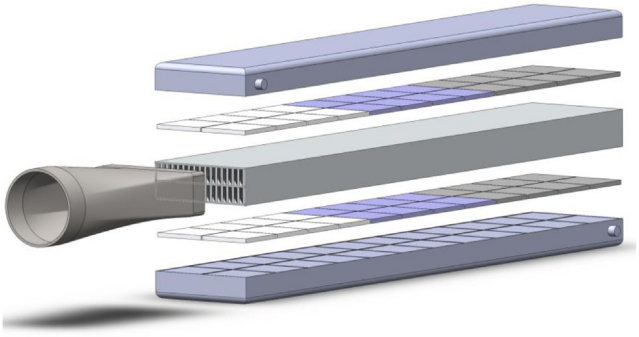

Fig. 9 – The final optimal architecture of the TEG subsystem.

subsystem. Module type is Melcor HT8. All the TEG modules are electrically divided into 3 branches along the exhaust gas flow. The heat exchanger 'Pin-fin plate-fin, surface PF-4(F)' is installed. This subsystem configuration is the optimal choice for both on-design and off-design operating conditions. The procedures of optimizing the TE exhaust heat recovery subsystem are also clearly presented.

The electrical connection style of the TEG assembly is analyzed. It affects the subsystem in various aspects: the optimal size, the reliability and the performance, both on-design and especially off-design. In the end, balanced between the subsystem performance and complexity, 3-branch scenario is chosen. This increases the subsystem power output by 12.9%.

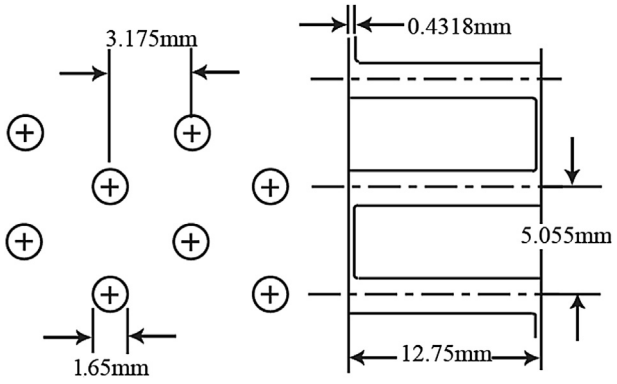

Fig. 10 – Detailed geometry of 'Pin-fin plate-fin, surface PF-4(F)'.

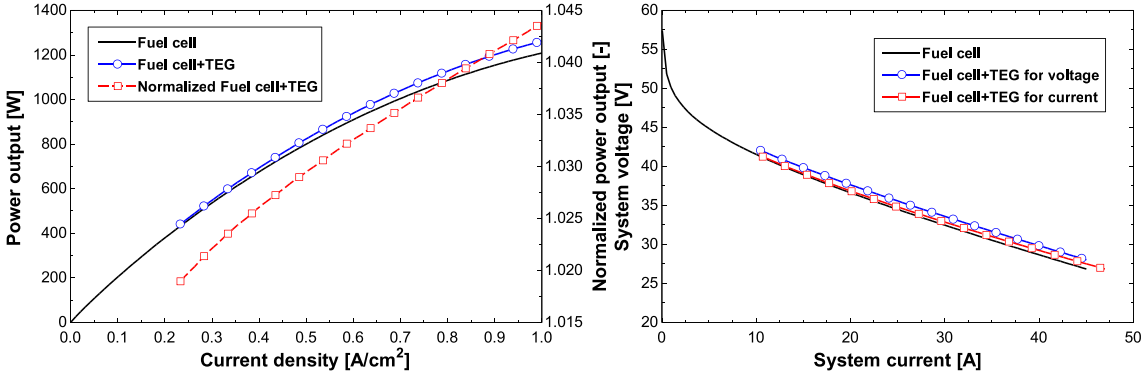

Fig. 11 – Contribution of TE heat recovery to the fuel cell system, ZT = 0.50.

It seems the possible TEG–TEC working mode shift in the current subsystem should also be included in simulating its performance. The current TEG system-level model widely used in literature probably overestimates the subsystem performance when large temperature unevenness happens among modules.

The current TEG modules of the subsystem only have a ZT = 0.50. Under this condition, the subsystem can boost the fuel cell system power output by around 3.5%. With achievements in material science, this number can be expected up to 10% in the near future.

By now, the TEG subsystem for HT-PEM fuel cell exhaust heat recovery has been optimized through simulations. Practical concerns and the feasibility of deploying this TEG subsystem to increase the fuel cell system efficiency still need further experimental assessments. Larger scale system-level modeling and simulation study would also be beneficial.

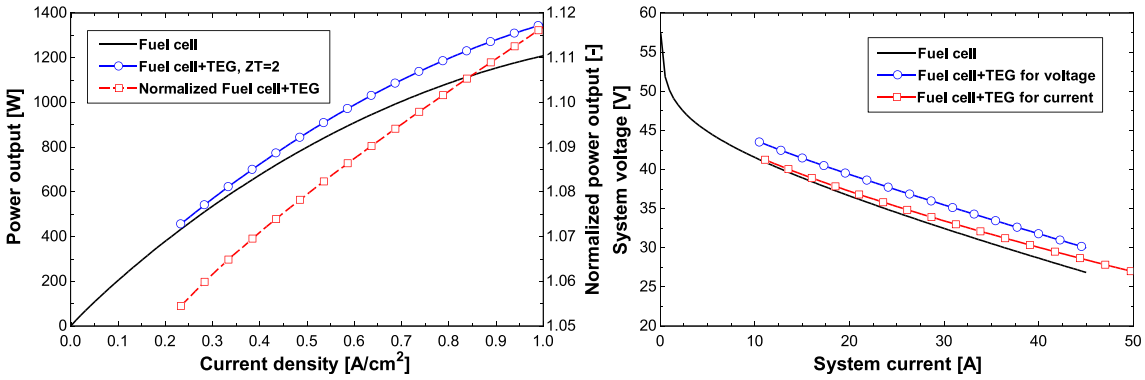

Fig. 12 – Expected contribution of TE heat recovery to the fuel cell system, ZT = 2.

Acknowledgments

The authors gratefully acknowledge financial support from Aalborg University and China Scholarship Council.

REFERENCES

[1] Cheddie Denver, Munroe Norman. Review and comparison of approaches to proton exchange membrane fuel cell modeling. J Power Sources 2005;147:72–84.
[2] Crabtree George W, Dresselhaus Mildred S, Buchanan Michelle V. The hydrogen economy. Phys Today 2004;57(12):39. http://dx.doi.org/10.1063/1.1878333.
[3] Quartarone Eliana, Mustarelli Piercarlo. Polymer fuel cells based on polybenzimidazole/H_3PO_4. Energy Environ Sci 2012;5:6436–44.
[4] Andreasen Søren Juhl, Ashworth Leanne, Menjon Remon Ian Natanael, Rasmussen Peder Lund, Nielsen Mads Pagh. Modeling and implementation of a 1 kW, air cooled HTPEM fuel cell in a hybrid electrical vehicle. ECS Trans 2008;12(1):639–50.
[5] Arsalis Alexandros, Nielsen Mads P, Kær Søren K. Application of an improved operational strategy on a PBI fuel cell-based residential system for Danish single-family households. Appl Therm Eng 2013;50(1):704–13.
[6] Advantages of HTPEM fuel cells over LTPEM fuel cells. http://www.serenergy.com/htpem_technology.htm.
[7] Andreasen Søren Juhl, Vang Jakob Rabjerg, Kær Søren Knudsen. High temperature PEM fuel cell performance characterisation with CO and CO_2 using electrochemical impedance spectroscopy. Int J Hydrogen Energy 2011;36:9815–30.
[8] Gao Xin, Andreasen Søren Juhl, Chen Min, Kær Søren Knudsen. Numerical model of a thermoelectric generator with compact plate-fin heat exchanger for high temperature PEM fuel cell exhaust heat recovery. Int J Hydrogen Energy 2012;37:8490–8.
[9] Gao Xin, Chen Min, Snyder G Jeffrey, Andreasen Søren Juhl, Kær Søren Knudsen. Thermal management optimization of a thermoelectric-integrated methanol evaporator using a compact CFD modeling approach. J Electron Mater 2013;42(7):2035–42.
[10] Gao Xin, Chen Min, Andreasen Søren Juhl, Kær Søren Knudsen. Potential usage of thermoelectric devices in a high-temperature polymer electrolyte membrane (PEM) fuel cell system: two case studies. J Electron Mater 2012;41(6):1838–44.
[11] Kays WM, London AL. Compact heat exchangers. 3rd ed. New York: McGraw Hill; 1984.
[12] Andreasen Søren Juhl, Ashworth Leanne, Menjón Remón Ian Natanael, Kær Søren Knudsen. Directly connected series coupled HTPEM fuel cell stacks to a Li-ion battery DC-bus for a fuel cell electrical vehicle. Int J Hydrogen Energy 2008;33(23):7137–45.
[13] Serenus 166/390 AirC Datasheet. http://www.serenergy.com/Downloads.htm [accessed: 22.10.12].
[14] Suzuki RO, Tanaka D. Mathematical simulation of thermoelectric power generation with the multi-panels. J Power Sources 2003;122(2):201–9.
[15] Suzuki RO, Tanaka D. Mathematic simulation on thermoelectric power generation with cylindrical multitubes. J Power Sources 2003;124(1):293–8.
[16] Mori M, Yamagami T, Oda N, Hattori M, Sorazawa M, Haraguchi T. Current possibilities of thermoelectric technology relative to fuel economy. Society of Automotive Engineering; 2009. 2009-2101-0170.
[17] Yu Chuang, Chau KT. Thermoelectric automotive waste heat energy recovery using maximum power point tracking. Energy Convers Manag 2009;50:1506–12.
[18] Jong-Pil Im, Se-Won Wang, Seung-Tak Ryu, Gyu-Hyeong Cho. A 40 mV transformer-reuse self-startup boost converter with MPPTcontrol for thermoelectric energy harvesting. IEEE Journal of Solid-State Circuits 2012;47(12):3055–67.
[19] Chatzidakis Panagiotis G, Christidis Georgios C, Tatakis Emmanuel C. Comparative study of MPPT algorithms for thermoelectric generators. In: 2013 15th European conference on power electronics and applications (EPE; 2013. http://dx.doi.org/10.1109/EPE.2013.6634607.
[20] Korsgaard Anders R, Refshauge Rasmus, Nielsen Mads P, Bang Mads, Kær Søren K. Experimental characterization and modeling of commercial polybenzimidazole-based MEA performance. J Power Sources 2006;162:239–45.
[21] Arsalis Alexandros, Nielsen Mads P, Kær Søren K. Modeling and off-design performance of a 1 kWe HT-PEMFC (high temperature-proton exchange membrane fuel cell)-based residential micro-CHP (combined-heat-and-power) system for Danish single-family households. Energy 2011;36:993–1002.
[22] Khattab NM, El Shenawy ET. Optimal operation of thermoelectric cooler driven by solar thermoelectric generator. Energy Convers Manag 2006;47:407–26.
[23] Meng Fankai, Chen Lingen, Sun Fengrui. Performance analysis for two-stage TEC system driven by two-stage TEG obeying Newton's heat transfer law. Math Comput Model 2010;52:586–95.
[24] Smith KD. An investigation into the viability of heat sources for thermoelectric power generation systems. Master thesis. Rochester (NY): Rochester Institute of technology; 2009.
[25] Snyder G Jeffrey, Toberer Eric S. Complex thermoelectric materials. Nat Mater 2008;7:105–14.
[26] Yang J, Stabler FR. Automotive applications of thermoelectric materials. J Electron Mater 2009;38(7):1245–51.
[27] Jovanovich V, Ghmaty S. Design, fabrication and testing of energy harvesting thermoelectric generator. In: Proc of SPIE, vol. 6173; 2006. pp. 1–8.